DRAFT VERSION OCTOBER 28, 2011
Preprint typeset using LaTeX style emulateapj v. 11/10/09

QATAR-2: A K DWARF ORBITED BY A TRANSITING HOT JUPITER AND A MORE MASSIVE COMPANION IN AN OUTER ORBIT

MARTA L. BRYAN[1], KHALID A. ALSUBAI[2], DAVID W. LATHAM[3], NEIL R. PARLEY[4], ANDREW COLLIER CAMERON[4], SAMUEL N. QUINN[3], JOSHUA A. CARTER[3,12], BENJAMIN J. FULTON[5], PERRY BERLIND[3], WARREN R. BROWN[3], LARS A. BUCHHAVE[6,8], MICHAEL L. CALKINS[3], GILBERT A. ESQUERDO[3], GÁBOR FŰRÉSZ[3,14], UFFE GRÅE JØRGENSEN[6,8], KEITH D. HORNE[4], ROBERT P. STEFANIK[3], RACHEL A. STREET[5], GUILLERMO TORRES[3], RICHARD G. WEST[7], MARTIN DOMINIK[4,13], KENNET B. W. HARPSØE[6,8], CHRISTINE LIEBIG[4], SEBASTIANO CALCHI NOVATI[9,10], DAVIDE RICCI[11], JESPER F. SKOTTFELT[6,8]

Draft version October 28, 2011

ABSTRACT

We report the discovery and initial characterization of Qatar-2b, a hot Jupiter transiting a V = 13.3 mag K dwarf in a circular orbit with a short period, P_b = 1.34 days. The mass and radius of Qatar-2b are $M_P = 2.49\,M_J$ and $R_P = 1.14\,R_J$, respectively. Radial-velocity monitoring of Qatar-2 over a span of 153 days revealed the presence of a second companion in an outer orbit. The Systemic Console yielded plausible orbits for the outer companion, with periods on the order of a year and a companion mass of at least several M_J. Thus Qatar-2 joins the short but growing list of systems with a transiting hot Jupiter and an outer companion with a much longer period. This system architecture is in sharp contrast to that found by *Kepler* for multi-transiting systems, which are dominated by objects smaller than Neptune, usually with tightly spaced orbits that must be nearly coplanar.

Subject headings: planetary systems — stars: individual (Qatar-2, 2MASS 13503740-0648145) — techniques: spectroscopic

1. INTRODUCTION

Wide-angle ground-based photometric surveys, such as WASP and HATNet, have been effective for the identification of close-in exoplanets that transit their host stars. Although most of the systems found by these surveys are fainter than the stars targeted by Doppler surveys, they are still bright enough to allow confirmation and characterization of their transiting planets using follow-up photometric and spectroscopic observations.

Most of the more than 150 confirmed transiting planets are hot Jupiters. Of those found by ground-based surveys, only 12 are smaller than Saturn, i.e. less than 9.4 Earth radii (Schneider 2011, as of September 2011). In contrast, most of the more than 1000 candidates identified by *Kepler* are smaller than Neptune, i.e. less than 3.8 Earth radii (e.g., see Latham et al. 2011). However, it will not be possible to determine spectroscopic orbits for the vast majority of *Kepler's* small candidates, because the required velocity precision is beyond the reach of present capabilities with instruments such as HIRES on Keck 1 (e.g., see Batalha et al. 2011).

Part of the problem is that most of the *Kepler* candidates are 14th magnitude or fainter, a result of the fact that *Kepler* monitors a region that is only 0.25% of the sky. To find all of the nearest and brightest transiting planets, we now need to extend our photometric surveys to cover the entire sky. The prospects are good that such surveys will eventually be pursued from space, with missions such as TESS (an Explorer selected for Phase A by NASA) and PLATO (proposed to ESA), but the earliest any of those spacecraft could be launched is 2016.

In the meantime, at least three teams are working on ground-based photometric surveys designed to find the best systems for follow-up studies. An obvious strategy is to cover as much of the sky as possible (idealy all), so that no prime systems are missed. A complementary strategy is to target smaller stars, where smaller planets are easier to detect and characterize. The MEarth project has adopted both strategies by focusing on the coolest and smallest M dwarfs, targeting a few thousand of the nearest and brightest examples all over the sky. This approach has already yielded GJ 1214b (Charbonneau et al. 2009), which lies in the "Super-Earth" transition region between Neptune and the Earth and has attracted a lot of interest because its favorable contrast with its host star allows studies of its atmosphere (e.g., see Bean et al. 2011). The other two efforts, the extensions of HATNet to HAT South and of WASP to the Qatar Exoplanet Survey (QES), have chosen to improve the capability of the more traditional strategy of a magnitude-limited wide-angle survey. Both HAT South and QES have implemented cameras with larger apertures, thus providing better photometric precision and lower rates of contamination by faint stars close to the targets (enabled by the more favorable pixel scale resulting from the longer focal lengths of the larger cameras). An important trade-off of this approach is that it requires more

[1] Department of Astronomy, Harvard University, Cambridge, MA 02138, USA
[2] Qatar Foundation, PO BOX 5825 Doha, Qatar
[3] Harvard-Smithsonian Center for Astrophysics, 60 Garden Street, Cambridge, MA 02138, USA
[4] SUPA, School of Physics and Astronomy, University of St Andrews, North Haugh, St Andrews, Fife KY16 9SS, UK
[5] Las Cumbres Observatory Global Telescope Network, 6740 Cortona Drive, Suite 102, Goleta, CA 93117, USA
[6] Niels Bohr Institute, University of Copenhagen, Juliane Maries vej 30, 2100 Copenhagen, Denmark
[7] Department of Physics and Astronomy, University of Leicester, Leicester LE1 7RH, UK
[8] Centre for Star and Planet Formation, Geological Museum, Øster Voldgade 5, 1350 Copenhagen, Denmark
[9] Università degli Studi di Salerno, Dipartimento di Fisica "E.R. Caianiello", Via S. Allende, 84081 Baronissi (SA), Italy
[10] INFN, Gruppo Collegato di Salerno, Sezione di Napoli, Italy
[11] Institut d'Astrophysique et de Géophysique, Allée du 6 Août 17, Sart Tilman, Bât. B5c, 4000 Liège, Belgium
[12] Hubble Fellow
[13] Royal Society University Research Fellow
[14] Konkoly Observatory of the Hungarian Academy of Sciences, Budapest, Hungary

detector pixels to cover the same area on the sky.

A practical implication of finding smaller planets is that the follow-up Doppler spectroscopy needed to determine orbits and planetary masses will demand access to the most capable facilities for very precise radial velocities, such as HARPS on the European Southern Observatory's 3.6-m telescope on la Silla in the South, and HARPS-N, scheduled to come into operation in 2012 on the Telescopio Nazionale Galileo (TNG) 3.6-m telescope operated for the Italian Institute of Astrophysics (INAF) on La Palma in the North.

In this paper we report the discovery and initial characterization of Qatar-2b, the second transiting planet from the Qatar Exoplanet Survey to be confirmed (for the first, see Alsubai et al 2011). Qatar-2b is especially interesting, because our radial-velocity monitoring shows that there is a second companion in the system with an orbital period of about a year and a mass of at least several M_J.

2. QES DISCOVERY PHOTOMETRY

The Qatar Exoplanet Survey (QES) is a wide-field photometric survey for transiting planets. The initial 5-camera CCD imaging system is now deployed at a site in New Mexico and has been in operation for more than two years. It uses an array of five Canon lenses equiped with 4K $\times$ 4K CCDs to image an $11^\circ \times 11^\circ$ field on the sky simultaneously at two different pixel scales (Alsubai et al 2011). The data are reduced at the University of St. Andrews using pipeline software based on the image-subtraction algorithm of Bramich (2008), and the data products are archived at the University of Leicester, using the same architecture as the WASP archive (Pollacco et al. 2006).

The QES photometry for the V = 13.3 mag K dwarf that we now designate Qatar-2 (3UC 167-129863, $\alpha_{2000} = 13^{\rm h}50^{\rm m}37\overset{\rm s}{.}41$, $\delta_{2000} = -06^\circ48'14\overset{''}{.}4$ (Zacharias et al. 2010)) revealed transit-like events, found by an automated search on the archive data using the box least-squares algorithm of Kovács, Zucker, & Mazeh (2002) as modified for the SuperWASP project by Collier Cameron et al. (2006). Systematic patterns of correlated noise were modeled and removed from the archive light curves using a combination of the SysRem algorithm of Tamuz, Mazeh, & Zucker (2005) and the trend filtering algorithm (TFA) of Kovács, Bakos, & Noyes (2005). 3UC 167-129863 was screened and selected as a promising candidate, along with two other stars in the same QES field, using tests described by Collier Cameron et al. (2007), designed to ensure that the depths and durations of observed transits are consistent with the expectations for objects of planetary dimensions transiting main-sequence stars. The discovery light curve, shown in Figure 1, indicated an ephemeris of $E = 2455618.9092 \pm 0.0014 + N \times 1.337098 \pm 0.000022$ BJD. The final photometric data for the QES light curves are provided in full in the electronic version of the journal.

3. FOLLOW-UP SPECTROSCOPY WITH TRES

We monitored the spectrum of Qatar-2 using the Tillinghast Reflector Echelle Spectrograph (TRES), mounted on the 1.5m Tillinghast Reflector at the Fred L. Whipple Observatory on Mount Hopkins, Arizona. Over a period of 153 days from 2011 January 18 to June 21 we obtained 44 spectra with a signal-to-noise ratio per resolution element (SNRe) of at least 20 in the continuum at the center of the order containing the Mg b features (near 518 nm). We used the medium fiber, which yields a resolving power of $R \sim 44,000$, corresponding to a resolution element with 6.8 km s^{-1} FWHM. The spectra were extracted using the procedures outlined by Buchhave et al. (2010). The wavelength calibration was established using exposures of a Thorium-Argon hollow-cathode lamp illuminating the fiber, immediately before and after the stellar observations. A typical exposure time for a stellar observation was 45 minutes.

3.1. *Radial Velocities*

We derived radial velocities from the TRES spectra using the procedures for multi-order cross correlations described by Buchhave et al. (2010). We present here a brief summary of the technique. First, we rejected roughly half of the echelle orders: several orders with low SNR shortward of 446 nm; orders longward of 678 nm, which are contaminated by telluric absorption lines or show strong fringing in the CCD; and a few orders in between which are known to give poor velocity performance relative to the other orders (generally because of some other contamination such as interstellar Na D absorption or emission lines from the Earth's atmosphere). In all, we included 23 orders in our analysis. Each observed spectrum was cross correlated, order by order, against the corresponding orders from the strongest single observation, the one obtained on JD 2455646. The cross correlation functions (CCFs) from the individual orders were summed and fit with a Gaussian function to determine the radial velocity. We estimated the internal precision of the radial velocity for each observation by fitting a Gaussian to the CCFs of the individual orders and using the deviations from the global fit to calculate the standard deviation of the mean.

We adjusted the velocities to correct for small shifts in the zero point between observing runs, which mostly resulted from minor modifications to the hardware between some runs. We observed IAU radial-velocity standard stars every night and were able to establish the run-to-run shifts with an uncertainty on the order of 5 m s^{-1}. These adjustments have been applied to the individual velocities for Qatar-2 reported in Table 1, which are relative to the observation obtained on JD 2455646. The absolute velocity of that observed template was derived using our observations of IAU radial-velocity standard stars and correlations of the Mg b order against a library of synthetic templates, yielding a value of -23.8 ± 0.1 km s^{-1} on a system where the velocity of our primary standard, HD 182488, is defined to be -21.508 km s^{-1}. The error estimate for this absolute velocity is fairly large, because only a single echelle order was used in the comparison with HD 182488 by way of the synthetic library spectra, and the absolute velocity of HD 182488 itself has an uncertainty at the level of nearly 0.1 km s^{-1}.

3.2. *Orbital Solution*

We ran a Markov Chain Monte Carlo (MCMC) analysis on the radial velocity data, starting with Gaussian constraints on the priors for period and epoch from the QES discovery photometry. We found that a single Keplerian orbit matched the data poorly, with $\chi^2 = 424.9$ for 44 observations and 38 degrees of freedom. Introducing two additional terms, for a linear and quadratic velocity drift in a Taylor expansion, resulted in a dramatic improvement to the fit, with $\chi^2 = 46.0$ for 36 degrees of freedom (reduced $\chi^2 = 1.28$). This model provided convincing evidence that Qatar-2 is orbited by a transiting hot Jupiter, Qatar-2b, with period P = 1.34 days, plus a second companion, Qatar-2c, with a period of roughly a year. The velocity curves for the orbit of Qatar-2b (phased

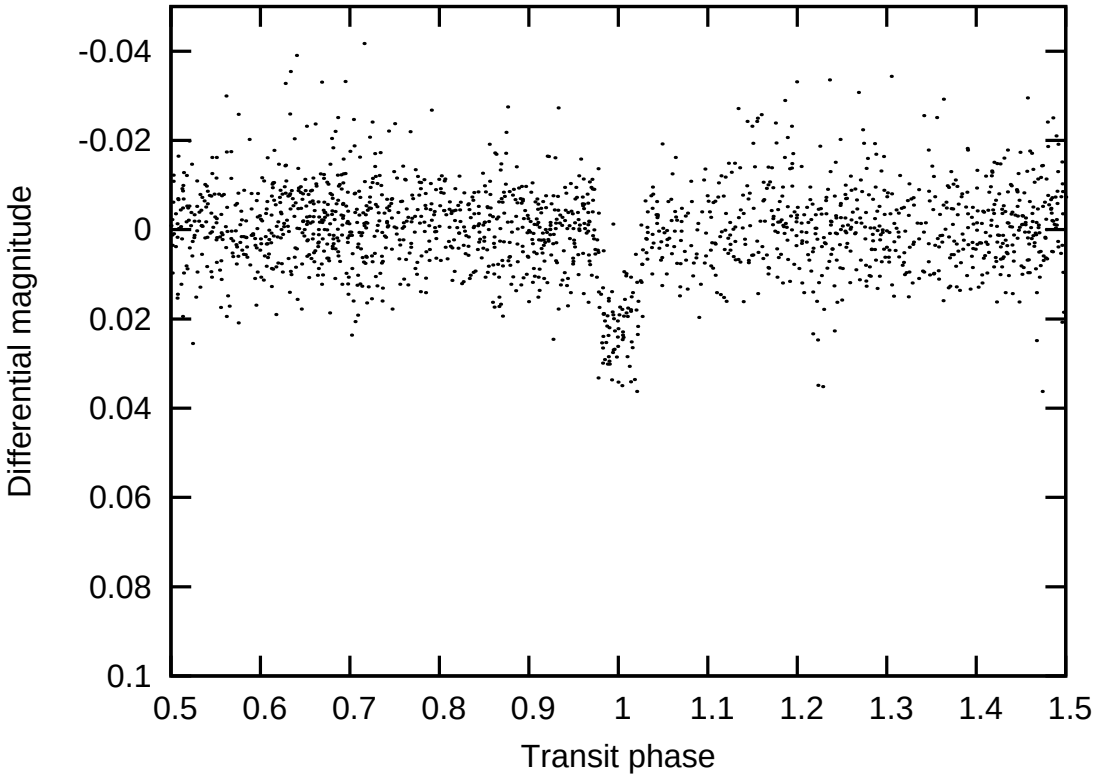

FIG. 1.— QES discovery light curve, phased on the transit ephemeris of Qatar-2b. The data shown here were obtained with Camera 403 in campaigns C2, C3 and C4.

to the period) and the acceleration due to Qatar-2c are plotted in the bottom two sections of Figure 2, together with the corresponding components of the observed velocities. The top panel shows the original velocities together with the combined velocity model. The panels immediately under the velocity curves show the residuals from the fits.

Next we used the Systemic Console (Meschiari et al. 2009) to explore possible simultaneous fits for two Keplerian orbits. A Levenberg-Marquardt solution gave a plausible fit and provided starting parameters for an MCMC analyis. When the eccentricities were allowed to be free parameters, several plausible solutions with similar parameters were found, all with periods a little shorter than a year and companion masses of several M_J. The key parameters for a typical solution from the Systemic Console are reported in Table 2, along with the parameters from the quadratic solution. Note that the period of the inner orbit from the radial velocities alone, $P_{RV} = 1.337169 \pm 0.000076$ is a close match to the period from the final global solution together with all the photometry, $P = 1.3371182 \pm 0.0000037$ days. A reliable solution of the orbit of Qatar-2c will require additional observations, which are planned for the coming season.

3.3. *Bisector Analysis*

The radial velocity of a star is defined to be the velocity of the center of mass of the star along the line of sight. Observationally, radial velocities are determined by measuring the Doppler shifts of spectral lines formed in the star's atmosphere. Distortions of line profiles due to phenomena such as dark spots on the surface of a rotating star or contamination of the spectrum by another star with variable velocity can mimic radial-velocity variations in the target star. A common technique for detecting line profile variations involves measurements of line bisector spans (e.g., see Queloz et al. 2001; Torres et al. 2007). Any variation in the bisector spans that is correlated with variations in the radial velocities is a strong warning that the velocity variation is probably not due to the reflex motion induced by an orbiting planet.

The variations in the bisector spans that we measured for the 44 TRES observations of Qatar-2 are reported in Table 1 and are plotted in the bottom panels of Figure 2. We were particularly interested to see if the bisector spans showed a correlation with the quadratic drift attributed to Qatar-2c, as might be expected if the outer companion contributed significant light. That would be compelling evidence that Qatar-2c was actually a star. No such trend is apparent in the bisector spans. There is also no correlation with the period of Qatar-2b, supporting the planet interpretation.

3.4. *Stellar Parameter Classification (SPC)*

The TRES spectra were also used to classify the stellar parameters of Qatar-2 using SPC, a new tool (Buchhave et al. in preparation) for comparing an observed spectrum with a library of synthetic spectra. SPC has its origins in the procedures developed for the analysis of spectra obtained with the CfA Digital Speedometers (cf. Carney et al. 1987; Latham et al. 2002). It is designed to solve simultaneously for effective temperature ($T_{\rm eff}$), metallicity ([m/H]), surface gravity ($\log g$), projected rotational velocity ($v \sin i$), and radial velocity (RV), taking advantage of the higher quality and more extensive wavelength coverage of the spectra produced by modern CCD echelle spectrographs. In essence, SPC cross-correlates an observed spectrum with a library of synthetic spectra for a grid of Kurucz model atmospheres and finds

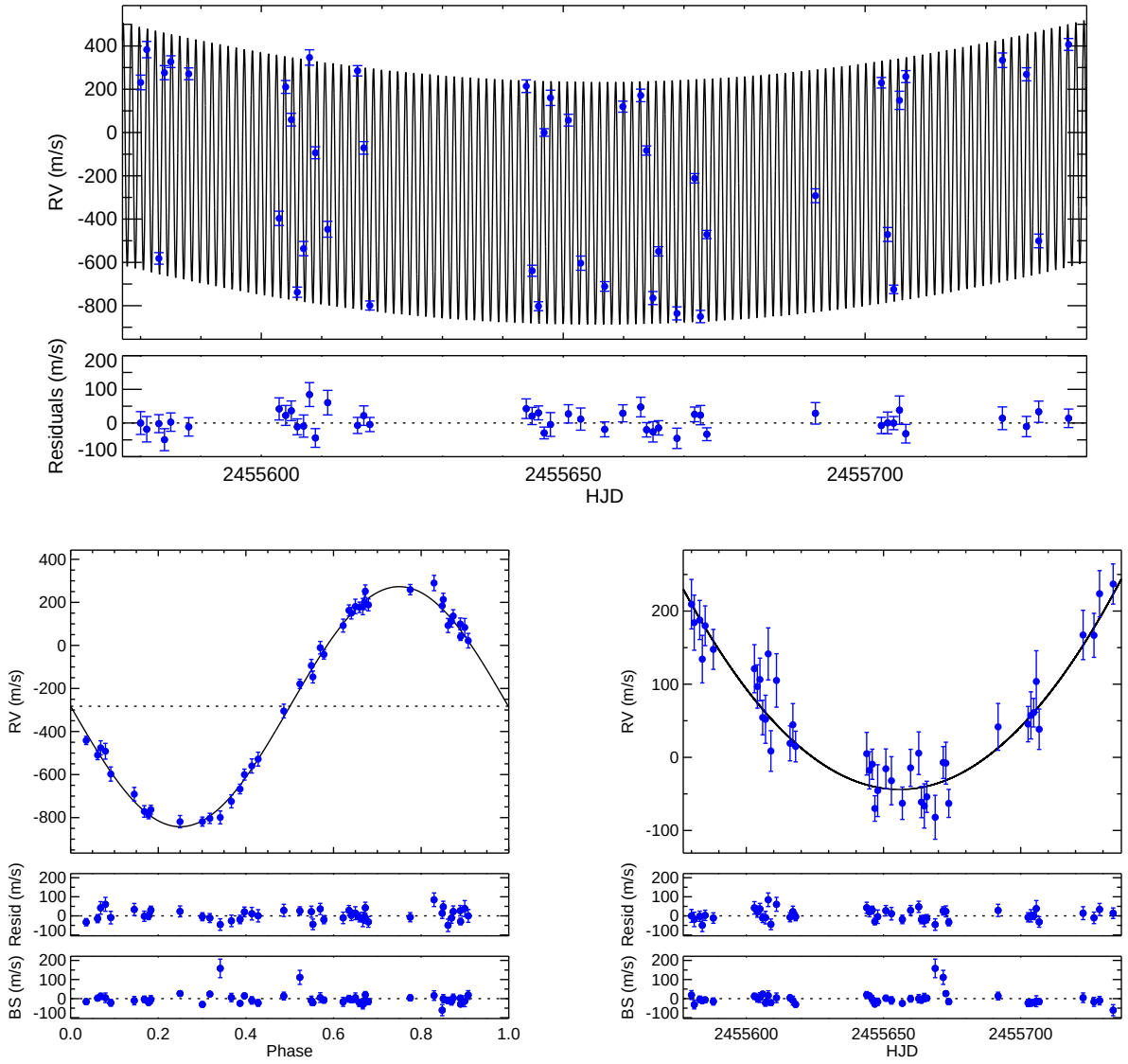

FIG. 2.— The velocity curve for the orbit of Qatar-2b (on the bottom left, phased to the period from the orbital fit) and for the quadratic residuals due to Qatar-2c (on the bottom right), together with the corresponding observed velocities. The top panel shows the original velocities together with the combined velocity model. The panels immediately under the velocity curves show the residuals from the fits. The variations in the bisector spans are plotted in the very bottom panels.

the stellar parameters by determining the extreme of a multi-dimensional surface fit to the peak correlation values from the grid.

For the SPC analysis of Qatar-2 we shifted the 44 observed spectra to a common velocity and co-added them, to obtain a combined observed spectrum with SNRe of 175 in the continuum near the Mg b features at 518 nm. An SPC analysis yielded $T_{\rm eff}$ = 4610 ± 50 K, $\log g$ = 4.65 ± 0.10 (cgs), [m/H] = –0.02 ± 0.08, and $v \sin i$ = 2.8 ± 0.5 km s^{-1}. The errors quoted here are our best guesses at the limit set by the systematic errors, which dominate the internal errors estimated from the consistency of the results for the individual observations. These values of $T_{\rm eff}$ and [m/H] are inputs to the determination of the mass and radius of the host star (not to mention its age) using stellar models, as described in section 6. This is an important issue, because the accuracy of the mass and radius determined for a transiting planet is often limited by uncertainties in the mass and radius of its host star.

4. FOLLOW-UP PHOTOMETRY

4.1. *KeplerCam Observations*

Light curves for four transits of Qatar-2b were obtained by use of KeplerCam on the 1.2 m telescope at the Fred Lawrence Whipple Observatory on Mount Hopkins, Arizona. KeplerCam utilizes a single Fairchild 486 4K × 4K CCD to cover an area of 23′ × 23′ on the sky, with a typical FWHM of 2.″5 for stellar images. We observed transit events of Qatar-2b on the nights of 2011 February 26, 2011 March 6, 2011 March 14, and 2011 March 18. The number of images captured for each of these events was 79, 109, 94, and 168 respectively. An SDSS *i*-band filter was used for three of the transits, and an SDSS *g*-band filter was used for the fourth. For one of the *i*-band light curves we only covered half a transit, due to increasing cloud cover around the time of egress. The *g*-band light curve was acquired in order to look for possible color effects due to light from additional stars contaminating the Qatar-2 image, such as a background eclipsing binary.

TABLE 1
RELATIVE RADIAL VELOCITIES OF QATAR-2.

BJD	RV[a] ($m s^{-1}$)	σ_{RV}[b] ($m s^{-1}$)	BS[c] ($m s^{-1}$)	σ_{BS} ($m s^{-1}$)
2455580.011622	231.4	33.8	18.8	23.2
2455581.027117	383.2	37.7	–31.5	22.6
2455583.034587	–581.6	26.7	–3.8	16.8
2455583.961503	276.4	32.6	–9.7	17.1
2455585.003598	327.3	27.2	–6.7	13.8
2455587.983438	271.2	27.4	–15.0	18.6
2455602.958910	–396.5	32.9	12.2	16.0
2455604.034894	210.7	29.6	2.7	21.0
2455604.966229	59.3	29.2	5.3	25.4
2455605.966418	–737.8	23.6	23.7	12.3
2455607.001348	–536.2	32.9	–22.0	18.0
2455607.987854	346.7	35.5	15.8	25.2
2455608.955271	–93.6	27.7	–21.6	14.9
2455610.996605	–447.0	36.5	4.2	25.2
2455615.938163	285.1	23.9	3.8	15.8
2455616.973605	–71.0	28.9	–10.2	23.1
2455617.978176	–799.2	21.0	–30.7	13.6
2455643.881697	214.0	29.1	19.7	17.1
2455644.849974	–638.7	25.5	14.6	12.6
2455645.901592	–802.6	20.6	–4.8	20.6
2455646.846694	0.0	17.4	–28.8	11.6
2455647.890953	160.3	35.4	–16.8	19.1
2455650.857343	57.0	27.1	2.1	15.3
2455652.895515	–603.6	32.9	–9.2	19.4
2455656.870962	–711.0	22.2	–25.0	10.9
2455659.877783	119.4	25.4	–0.8	17.5
2455662.839965	171.5	29.1	–0.4	21.5
2455663.812865	–83.3	21.3	–7.8	15.6
2455664.867650	–764.9	30.3	5.6	21.7
2455665.796571	–549.1	21.3	2.3	14.6
2455668.845188	–835.7	30.1	158.4	48.5
2455671.762510	–211.4	21.8	111.4	36.9
2455672.733966	–850.1	28.6	26.5	13.1
2455673.784772	–471.2	19.2	–16.2	14.9
2455691.770974	–292.0	32.0	13.4	20.3
2455702.699240	229.8	24.2	–22.9	19.0
2455703.727260	–471.1	32.2	–22.6	17.6
2455704.730193	–724.7	19.5	–20.6	12.5
2455705.694921	148.7	42.0	–13.7	28.5
2455706.738098	258.4	27.6	–15.8	15.8
2455722.744329	334.0	33.7	4.6	25.0
2455726.718494	269.1	30.1	–16.9	23.6
2455728.755461	–500.9	31.5	–10.7	22.1
2455733.706680	407.0	27.5	–60.7	28.9

[a] The zero-point of these velocities is relative to the observation obtained on BJD 2455646. The absolute velocity of that observation on the IAU system is $-23.8 \pm 0.1\,km\,s^{-1}$

[b] Internal errors, summed in quadrature with the uncertainty of the run-to-run zero point shifts, assumed to be $5\,m\,s^{-1}$.

[c] The zero point of the bisector spans is arbitrary.

TABLE 2
KEY ORBITAL PARAMETERS

Parameter	Quadratic	Systemic[a]
P_b (days)	1.337169 ± 0.000076	1.337148 ± 0.000095
K_b ($m\,s^{-1}$)	559 ± 6	559 ± 6
M_b (M_J)	2.48 ± 0.03	2.49 ± 0.05
e_b	0.01 ± 0.01	0.003 ± 0.008
P_c (days)	.....	332::
K_c ($m\,s^{-1}$)	.....	301::
M_c (M_J)	.....	8.4::
e_c	.....	0.09::
$\Delta\gamma$[b] ($m\,s^{-1}$)	-282.6 ± 5.2	.....
$d\gamma/dt$ ($m\,s^{-1}d^{-1}$)	-2.76 ± 0.16	.....
$d^2\gamma/dt^2$ ($m\,s^{-1}d^{-2}$)	0.0875 ± 0.0046	.....

[a] This is a typical solution from the Systemic Console; we do not quote errors for the parameters of the outer orbit, because the Systemic Console yielded several plausible solutions, with differences much larger than the internal error estimates. The parameters given here for the outer companion should be treated with extreme caution.

[b] $\Delta\gamma$ is the offset of the center-of-mass velocity for the set of relative velocities used for the orbital solution and reported in Table 1

The goal of the KeplerCam observations was to produce high-quality light curves, model them, and derive values for the radius ratio of the planet to the star, $R_P/R_\star$; the scaled semi-major axis of the orbit, $a/R_\star$; and orbital inclination, i (or equivalently the impact parameter, b). Differential aperture photometry was carried out on the images, after the usual steps of bias subtraction and flat-fielding. We experimented with the sizes used for the aperture for the stellar images and the annulus used for the sky subtraction. A smaller aperture reduces the contribution of sky background to the noise, but risks larger systematic errors due to imperfect centering of the stellar image. We chose the aperture and annulus sizes that gave the best balance between these two competing sources of error; $8''$ to $9''$ in diameter for the stellar aperture, and an annulus between $30''$ and $60''$ for the sky. Sections of the out-of-transit light curves that showed contamination by incoming clouds or dawn were rejected. Nine reference stars were identified, and the sum of their light curves was divided into the light curve for Qatar-2 in order to correct for atmospheric and instrumental effects. A linear trend was then fit to the out-of-transit sections of the resulting differential light curve and was used to normalize the light curve for Qatar-2b to unity.

Figure 3 shows the KeplerCam light curves together with the model fits described in section 6. The residuals of the photometric data from the model light curves are plotted below the light curves and show very little correlated noise. In addition, plots of the data against column and row position on the CCD showed no obvious correlation, and thus are not reproduced here. The final photometric data for the KeplerCam light curves are provided in full in the electronic version of the journal.

4.2. *LCOGT Observations*

Four partial transit events were observed with a 0.8m telescope operated by the Las Cumbres Observatory Global Telescope (LCOGT) at the Byrne Observatory at Sedgwick Reserve (BOS) near Santa Ynez, CA. The Sedgwick telescope is equipped with a Santa Barbara Instrument Group STL-6303E camera utilizing a $3K \times 2K$ Kodak Enhanced KAF-6306E CCD with a pixel scale of $0.572''$ per pixel (2×2 binning), and a $14.7' \times 9.8'$ field of view. We observed in the SDSS r band with exposure times of 120s.

The images were reduced using standard routines for bias subtraction, dark current subtraction, and flat-field correction. We extracted instrumental fluxes for the stellar images using PyRAF and aperture photometry. Relative light curves were produced by dividing the fluxes of the target star by the sum of the fluxes of four comparison stars in each image. Each transit event was normalized to the out-of-transit flux on that particular night. Julian dates of mid-exposure were recorded during the observations, and later converted to BJD TDB using the online versions of the tools described by Eastman et al. (2010). Aperture sizes, between $4''$ and $7''$ depending on the image quality, were chosen in order to minimize the photometric residuals in the resulting light curves. The final photometric data for the LCOGT light curves are provided in full in the electronic version of the journal.

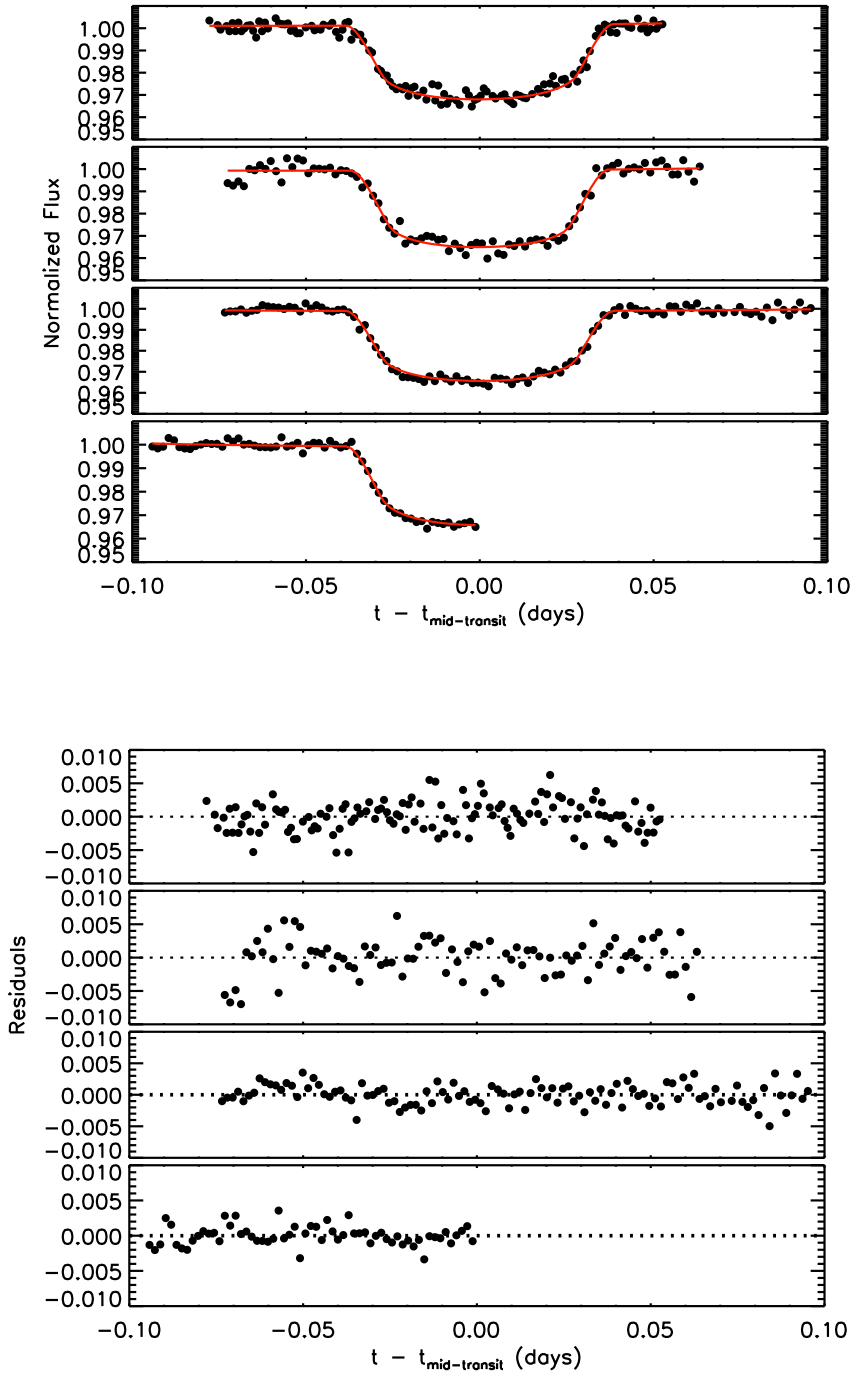

FIG. 3.— KeplerCam light curves for the transits of Qatar-2b. The second light curve from the top was obtained with an SDSS *g* filter, the other three were obtained with an SDSS *i* filter. The residuals from the model are shown underneath the light curves. The exposure times were 120 seconds for the *g* band and 60 for the *i* band.

5. HIGH-RESOLUTION IMAGES

A common source of astrophysical false positives for planet candidates discovered by wide-angle photometric surveys is contamination of the target image by an eclipsing binary, either by a physical companion in a hierarchical system or by an accidental alignment with a background binary. Ground-based surveys that utilize cameras with short focal lengths are particularly vulnerable to this problem, because the detector pixels typically span $10''$ or more on the sky. The 400mm focal-length Canon lenses used by the QES cameras produce images with a typical FWHM of $7\farcs5$. This is roughly half the size of the images produced by the 200mm Canon lenses used by several ground-based surveys, and thus the rate of contamination by background eclipsing binaries should be four times better. The images of the KeplerCam follow-up photometry have a typical FWHM of $2\farcs5$, so this should provide nearly an order of magnitude additional improvement in the contamination rate.

To push to even lower limits, we obtained high-resolution images with the Danish 1.54m telescope at the European Southern Observatory on La Silla, by use of an Andor iXon^{EM}+ 897 camera with an EMCCD chip, often called a Lucky-Imaging-camera because of its ability to obtain diffraction-limited images by recording lots of short exposures and collecting together the best images. The camera has a pixel size corresponding to $0\farcs09$, and was read at a frame rate of 10 Hz. In order to reach diffraction-limited images, one would usually stack the few percentage best quality images from a sequence, but here we have just applied the shift and add technique to all the images in a sequence of 1,000 individual exposures, which typically will reduce the seeing by a factor of about 3 compared to traditional CCD observations with the same total exposure time.

Figure 4 shows two of the resulting images. Qatar-2 is the bright star in the upper right part (i.e. north-west) of the images. The two fainter stars in the lower part of the image approximately $36''$ south-west of Qatar-2 are separated by slightly less than $0.6''$. The FWHM of the image of Qatar-2 is about $0\farcs5$, so these images reduce the area on the sky that could be contaminated by a background eclipsing binary by nearly another order of magnitude compared to the KeplerCam images. Although these images reduce the chance of a false positive due to a background eclipsing binary to a negligible level, they do not reduce significantly the chance of a false positive due to contamination in a hierarchical system, because the angular separation of most such systems is below the resolution of these images.

6. PHYSICAL CHARACTERISTICS OF THE STAR AND INNER PLANET

The stellar mass and radius for Qatar-2 were initially estimated using the values of $T_{\rm eff}$ and [m/H] derived from the spectra using SPC and the value for $a/R_\star$ derived from the KeplerCam light curves, together with isochrones from the Yonsei-Yale series of stellar models (Yi et al. 2001), following the procedures described by Torres et al. (2008). This yielded a mass of $M_\star = 0.742 \pm 0.35 M_\odot$, which was then imposed as an MCMC parameter controlled by a Gaussian prior on the simultaneous fit to the radial velocities and all the light curves from the QES, KeplerCam, and LCOGT photometry. All of our exploratory fits to the radial velocities indicated that the orbital eccentricity for Qatar-2b was indistinguishable from circular, so in our final model we fixed that eccentricity to zero and fit the residuals of the radial velocities from a circular orbit using a quadratic Taylor expansion. The transit light curves were modeled using the formulation of Mandel & Agol (2002) in the small-planet approximation. A four-coefficient nonlinear limb-darkening model was used, employing fixed coefficients appropriate to the *R* band for the QES photometry, the SDSS *r* band for the LCOGT photometry, and the SDSS *i* or *g* band for the KeplerCam photometry. These coefficients were determined from the tables of Claret (2004), interpolated to the values of $T_{\rm eff}$ and [m/H] determined from the TRES spectra using SPC.

The parameter optimization was performed using the current version of the MCMC code described by Collier Cameron et al. (2007) and Pollacco et al. (2008). The transit light curve is modeled in terms of the epoch T_0 of mid transit, the orbital period P, the ratio of the radii squared $d = (R_{\rm P}/R_\star)^2$, the approximate duration t_T of the transit from initial to final contact, and the impact parameter $b = (a\cos i)/R_\star$. The radial-velocity model is defined by the stellar orbital velocity semi-amplitude due to the inner planet K_b and three coefficients in a quadratic Taylor expansion for the acceleration of the star due to the outer planet, the first coefficient being the offset of the center-of-mass velocity for the relative velocities used for the orbital solution, $\Delta\gamma$. The values of $T_{\rm eff}$ and [m/H] were treated as additional MCMC parameters, constrained by Gaussian priors with mean values and variances as determined from the TRES spectra using SPC. The final light curves and corresponding fits from the global analysis are shown in Figure 5 for the QES discovery photometry and for the KeplerCam and LCOGT follow-up photometry. The correlations between the various posterior parameter estimates are shown in the matrix of plots in Figure 6. The final physical and orbital parameters and error estimates for the star and planet are reported in Table 3. It is reassuring to see the good agreement between the stellar parameters estimated from the spectra using SPC and the final values from the global analysis: $T_{\rm eff} = 4650 \pm 50$ K from SPC compared to 4645 ± 50, and $\log g = 4.65 \pm 0.10$ cgs versus 4.601 ± 0.018.

7. DISCUSSION

7.1. *Hot Jupiters with Companions*

One of the most important results from the *Kepler* mission is the discovery of a rich population of multiple transiting planets in systems whose orbits must be coplanar within a degree or two (Latham et al. 2011; Lissauer et al. 2011). Especially striking is the very low occurrence rate for hot Jupiters in the multiple systems found by *Kepler*. In the sample of 1235 planet candidates announced by Borucki et al. (2011), there are 117 systems that contain a planet candidate more massive than Saturn ($M_{\rm P} > 0.3 M_{\rm J}$) in an orbit with period shorter than 10 days, but only five of these systems harbor an additional transiting planet candidate. The remaining 112 transiting hot Jupiters are all in singles.

The occurrence rate is also very low for companions to hot Jupiters found by ground-based surveys, both photometric and spectroscopic. A review of the Extrasolar Planet Encyclopaedia (Schneider 2011) reveals that Qatar-2b joins HAT-P-13b, HAT-P-17b, and HAT-P-31b as the fourth transiting hot Jupiter with a confirmed outer planet, while only four hot Jupiters found by radial velocities have outer companions (HD 217107b, HIP 14810b, HD 187123b, and υ Andb). Of course, additional radial-velocity monitoring may reveal other hot Jupiters with outer companions, and there are al-

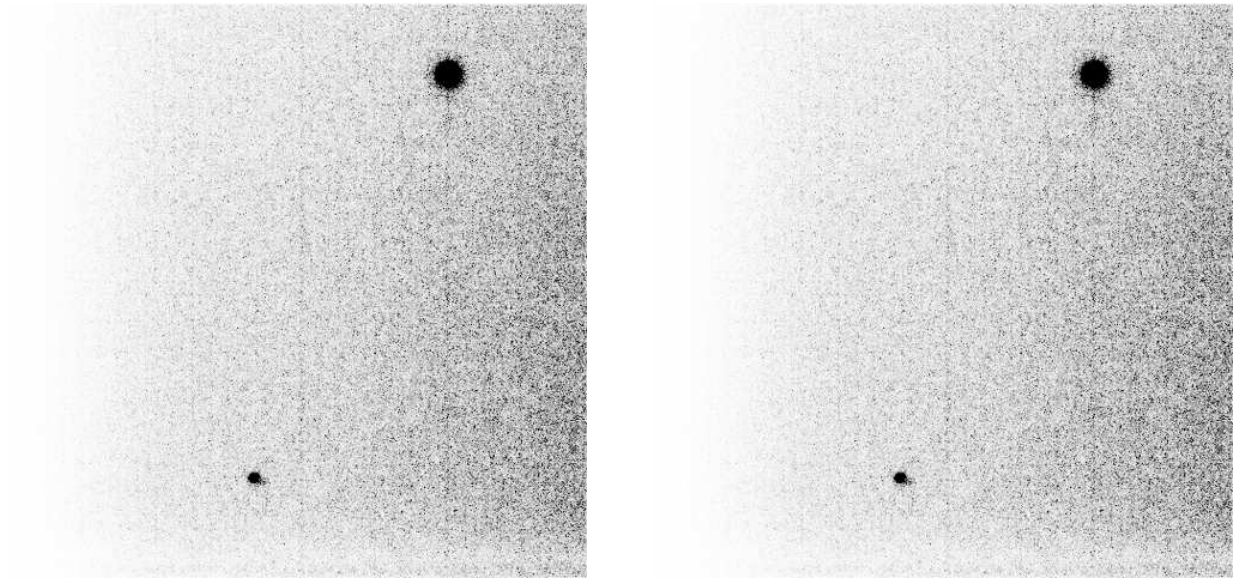

FIG. 4.— Lucky camera images of Qatar-2. North is up and west is left. The faint pair of stars 36″ to the south-west are separated by slightly less than 0.″6

TABLE 3
PLANETARY AND STELLAR PARAMETERS.

Parameter	Symbol	Value	Units
Transit epoch (BJD TDB)	T_0	$2455624.26679 \pm 0.00011$	days
Orbital period	P_b	1.3371182 ± 0.0000037	days
Transit duration	t_T	0.07540 ± 0.00049	days
Planet/star area ratio	$(R_P/R_\star)^2$	0.02725 ± 0.00040	
Impact parameter	b	0.19 ± 0.10	R_*
Scaled stellar radius	$R_\star/a$	0.1541 ± 0.0030	
Stellar density	$\rho_\star$	2.05 ± 0.12	$\rho_\odot$
Stellar effective temperature	$T_{\rm eff}$	4645 ± 50	K
Spectroscopic Metallicity	[m/H]	0 (fixed)	
Stellar surface gravity	$\log g_\star$	4.601 ± 0.018	(cgs)
Projected stellar rotation speed	$v \sin i$	2.8 (fixed)	$\mathrm{km\,s^{-1}}$
Stellar radius	$R_\star$	0.713 ± 0.018	$R_\odot$
Stellar mass	$M_\star$	0.740 ± 0.037	$M_\odot$
Orbital separation	a	0.02149 ± 0.00036	AU
Orbital inclination	i	88.30 ± 0.94	$^\circ$
Stellar reflex velocity	K_b	558.7 ± 5.9	$\mathrm{m\,s^{-1}}$
Center-of-mass velocity offset	$\Delta\gamma$	-282.6 ± 4.0	$\mathrm{m\,s^{-1}}$
Drift in center-of-mass velocity	$d\gamma/dt$	-2.74 ± 0.15	$\mathrm{m\,s^{-1}d^{-1}}$
Quadratic velocity drift term	$d^2\gamma/dt^2$	0.0870 ± 0.0043	$\mathrm{m\,s^{-1}d^{-2}}$
Orbital eccentricity	e	0 (fixed)	
Planet radius	R_p	1.144 ± 0.035	R_J
Planet mass	M_p	2.487 ± 0.086	M_J
Planet surface gravity	$\log g_p$	3.638 ± 0.022	(cgs)
Planet density	ρ_p	1.66 ± 0.13	ρ_J
Planetary equilibrium temperature	T_P	1292 ± 19	K

ready hints of velocity drifts for WASP-8 and WASP-22. All of the confirmed outer companions have relatively long orbital periods (see Table 4), so it is not surprising that none of them have shown transits, so far. Nevertheless, it is tempting to speculate that a close-in giant planet may stir up the orbits of other inner planets in its system, while a system of small planets is more likely to preserve the flatness of the disk from which it formed, allowing small planets to survive in surprisingly compact configurations.

In only one of the systems (HIP 14810) listed in Table 4 is the outer companion less massive than the hot Jupiter. In the rest of the systems the nearest companions are more massive, often by large factors.

7.2. *Orbits of Qatar-2b and HAT-P-31b*

Why is the orbit of HAT-P-31b eccentric, with $e = 0.2450 \pm 0.0045$ (Kipping et al. 2011), while the orbit of Qatar-2b is indistinguishable from circular? One possible explanation is that both orbits started out with significant eccentricity, perhaps as the result of a dynamical encounter that sent each planet on a path close to its host star, and the orbit of Qatar-2b has since been circularized by tidal forces, while the orbit of HAT-P-31b has not.

The circularization time scale goes something like $(M_P/M_\star)(a/R_\star)^5$. HAT-P-31b has a period of $P = 5.00$ days and mass of $M_P = 2.17 M_J$, orbits a late F star with mass

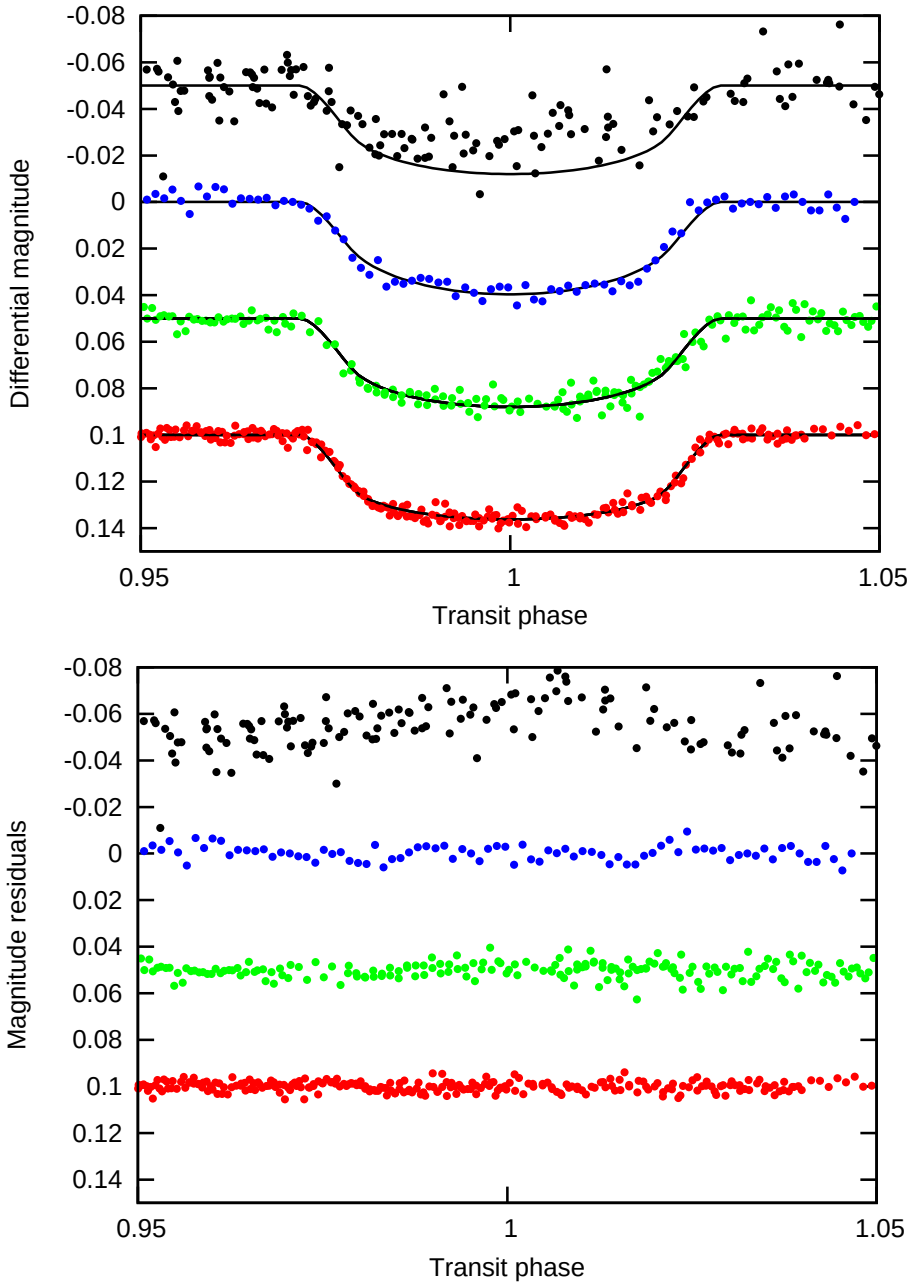

FIG. 5.— The fit of the light curves found by the global analysis. The first curve in the upper panel shows the QES discovery light curve in the *R* band; the second shows the KeplerCam SDSS *g*-band light curve; the third shows the LCOGT SDSS *r*-band light curve, and the fourth shows the KeplerCam SDSS *i*-band light curve. The lower panel shows the corresponding residuals from the global fit. The dip in the QES light curve may be too shallow due to aggressive detrending.

$M_\star = 1.22 M_\odot$, $a/R_\star = 8.9$, and is about 3 Gyr old. In contrast, Qatar-2b has a much shorter period of $P_b = 1.34$ days, similar mass of $M_P = 2.49 M_J$, orbits a K dwarf with mass of $M_\star = 0.74 M_\odot$, $a/R_\star = 6.3$, and is very likely a member of the Galactic disk. If Qatar-2 is three times older than HAT-P-31, the system age divided by the circularization time scale is nearly an order of magnitude longer for Qatar-2b, long enough so that there has been time for tidal forces to circularize the orbit. In addition, the host star for HAT-P-31b is close to the mass where the outer envelope no longer supports a convection zone, and the circularization time scale is even longer than implied by the simple relation that we adopted for the sake of this discussion.

Another effect that needs to be explored more carefully with dynamical simulations is the amount of eccentricity that Qatar-2c can pump into the orbit of Qatar-2b. Are the tidal forces working to circularize the orbit of Qatar-2b strong enough to keep the orbit circularized despite the perturbations from Qatar-2c? Finally, it would be interesting to estimate the size and patterns of the transit time variations expected for Qatar-2b due to perturbations by Qatar-2c.

7.3. *The Value of Deep Transits*

With a depth of about 3.5%, the transits of Qatar-2b are deeper than the transits of any other planet listed in The Extrasolar Planets Encyclopaedia (Schneider 2011). The clos-

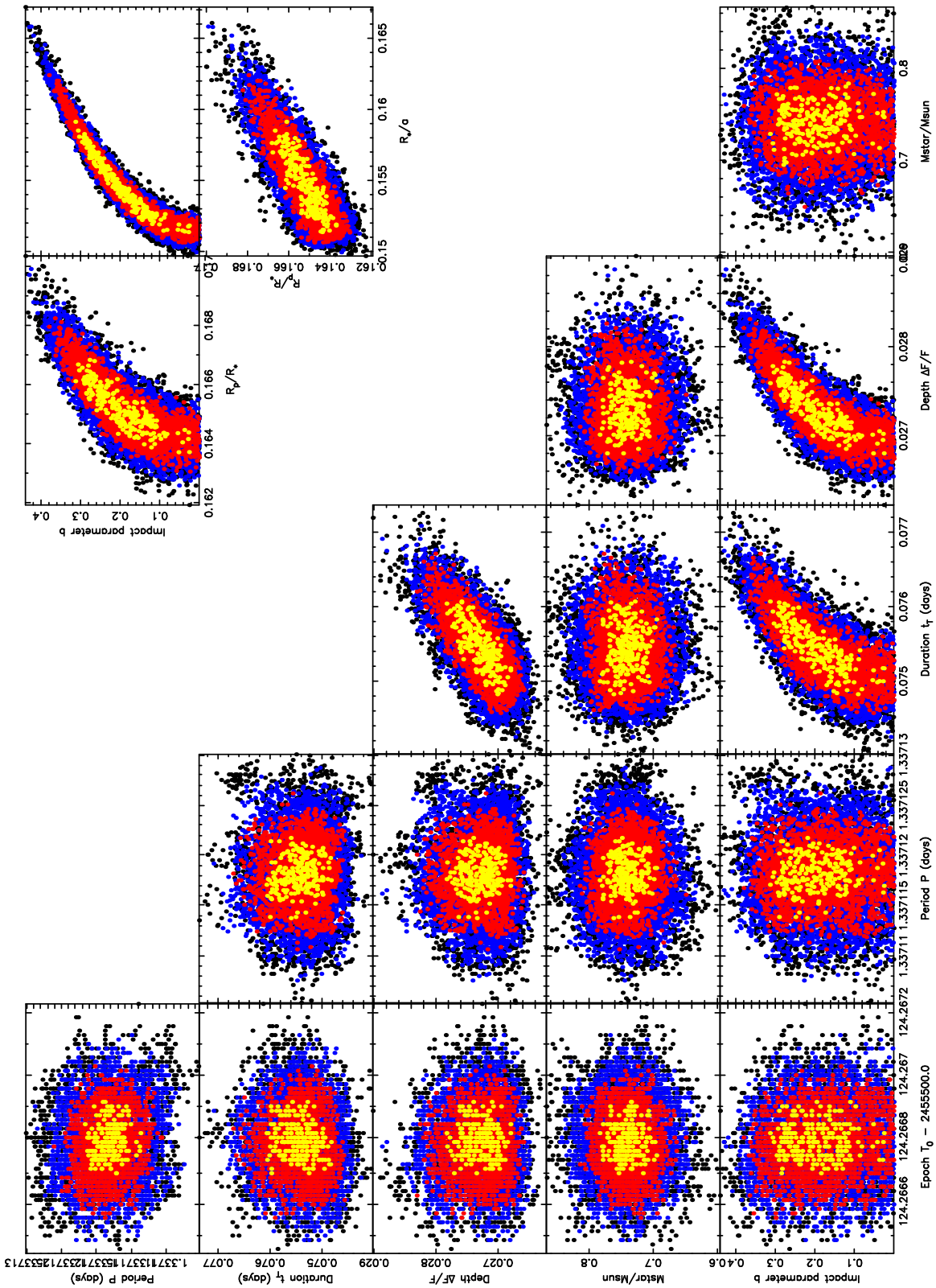

FIG. 6.— The correlations between the various posterior estimates from the MCMC global fit.

TABLE 4
HOT JUPITERS WITH COMPANIONS

Planet	$M_P(M_J)$[a]	$R_P(R_J)$	P (d)	a (AU)	e	i ($^\circ$)	$M_\star(M_\odot)$
Qatar-2b	2.49 ± 0.09	1.14 ± 0.04	1.337118	0.0215	0 (fixed)	88.30 ± 0.94	0.74
c	8.4::	.....	332::	0.82::	0.09::	.....	.....
HAT-P-13b	0.85 ± 0.04	1.28 ± 0.08	2.916243	0.0426	0.014 ± 0.05	83.3 ± 0.6	1.22
c	14.5 ± 1.0	.....	448.2 ± 1.0	1.19	0.67 ± 0.02	.....	.....
HAT-P-17b	0.53 ± 0.02	1.01 ± 0.03	10.338523	0.088	0.346 ± 0.007	89.2 ± 0.2	0.86
c	$1.4^{+1.1}_{-0.4}$	.....	1798^{+58}_{-89}	2.8	$0.1^{+0.2}_{-0.1}$	.....	.....
HAT-P-31b	$2.2^{\pm}0.1$	1.1 ± 0.4	5.005424	0.055	0.245 ± 0.005	$87.1^{+1.8}_{-2.7}$	1.22
c	> 3.4	.....	> 1022	.....	.....	.....	.....
HD 217107b	1.85 ± 0.05	.....	7.12689	0.073	0.132 ± 0.005	.....	1.02
c	2.5 ± 0.3	.....	4210 ± 190	5.27	0.52 ± 0.03	.....	.....
HIP 14810b	3.9 ± 0.3	.....	6.673855	0.069	0.1427 ± 0.0009	.....	0.99
c	1.3 ± 0.1	.....	147.73	0.55	0.16 ± 0.01	.....	.....
d	0.57 ± 0.05	.....	962 ± 15	1.9	0.17 ± 0.04	.....	.....
HD 187123b	0.52 ± 0.04	.....	3.0965828	0.043	0.01 ± 0.01	.....	1.06
c	2.0 ± 0.3	.....	3810 ± 420	4.9	0.25 ± 0.03	.....	.....
υ Andb	0.69 ± 0.03	.....	4.617136	0.059	0.013 ± 0.016	> 30	1.27
c	$14.0^{+2.3}_{-5.2}$	.....	240.94	0.83	0.245 ± 0.006	8 ± 1	.....
d	$10.3^{+0.7}_{-3.3}$	.....	1282	2.53	0.316 ± 0.006	24 ± 1	.....
e	1.06 ± 0.03	.....	3848	5.25	0.0054 ± 0.0004	.....	.....

[a] For the transiting hot Jupiters (the first four entries) the actual mass is reported; for the hot Jupiters discovered by Doppler surveys (the final four entries), the minimum mass is listed, except for υ And c&d, which are actual masses enabled by inclinations determined with the Fine Guidance Sensors on HST.

est rival is CoRoT-2b, with reported transit depths of 3.2% (Alonso et al. 2008). CoRoT-2 is a late G dwarf with $T_{\rm eff}$ = 5625 K, while Qatar-2 is a late K dwarf with $T_{\rm eff}$ = 4645 K; the smaller radius of Qatar-2 is the main reason for the deeper transits. A more interesting comparison may be the bright (V = 7.7 mag) early K dwarf HD 189733 with $T_{\rm eff}$ = 5050 K (cf. Bouchy et al. 2005; Bakos et al. 2006), which has been a favorite target for studies of the planet's atmosphere (cf. Knutson et al. 2007; Swain, Vasisht, & Tinetti 2008; Grillmair et al. 2008; Gibson, Pont, & Aigrain 2011). The contrast between the planet and host star is even more favorable for Qatar-2, but the system is much fainter (V = 13.3 mag). Thus HD 189733 is likely to continue as a top target for follow-up studies of hot Jupiters, although it may eventually be joined by other nearby bright transiting systems discovered by all-sky transit surveys such as TESS or PLATO, or by targeted searches of small cool stars such as MEarth. Nevertheless, Qatar-2 is a good target for amateurs and outreach projects such as MicroObservatory (http://mo-www.harvard.edu/MicroObservatory/) with telescopes of modest size but covering wide fields of view, because of the availability of many more reference stars of comparable magnitude.

G. F. acknowledges financial support from the Hungarian OTKA-NFU Mobility grant MB08C 81013. CL acknowledges the Qatar Foundation for support from QNRF grant NPRP-09-476-1-078. DR (boursier FRIA) acknowledges support from the Communauté française de Belgique - Actions de recherche concertées - Académie universitaire Wallonie-Europe. The Byrne Observatory at Sedgwick (BOS) is operated by the Las Cumbres Observatory Global Telescope Network and is located at the Sedgwick Reserve, a part of the University of California Natural Reserve System.

Facilities: TRES

REFERENCES

Alsubai, K. A., et al. 2011, MNRAS, in press (arXiv:1012.3027)
Alonso, R., et al. 2008, A&A, 482, L21
Bakos, G. Á., et al., 2006, ApJ, 650, 1160
Batalha, N. M., et al. 2011, ApJ, 729, 27
Bean, J. L., et al. 2011, ApJ, submitted (arXiv:1109.0582)
Borucki, W. J., et al. 2011 ApJ, 736, 19
Bouchy, F., et al. 2005, A&A, 444, L15
Bramich, D. M. 2008, MNRAS, 386, L77
Buchhave, L. A., et al. 2010, ApJ, 720, 118
Carney, B. W., Laird, J. B., Latham, D. W., & Kurucz, R. L. 1987, AJ, 93, 116
Charbonneau, D., et al. 2009, Nature, 462, 891
Claret, A. 2004, A&A, 428, 1001
Collier Cameron, A., et al. 2006, MNRAS, 373, 799
Collier Cameron, A., et al. 2007, MNRAS, 380, 1230
Eastman, J., Siverd, R., & Gaudi, B. S. 2010, PASP, 122, 935
Gibson, N., Pont., F., & Aigrain, S. 2011, MNRAS, 411, 2186
Grillmair, C., et al. 2008, Nature, 456, 767
Kipping, D. M., et al. 2011, AJ, 142, 95
Knutson, H., et al. 2007, Nature, 447, 183
Kovács, G., Bakos, G. Á., & Noyes, R. W. 2005, MNRAS, 356, 557
Kovács, G., Zucker, S., & Mazeh, T. 2002, A&A, 391, 369
Latham, D. W., Stefanik, R. P., Torres, G., Davis, R. J., Mazeh, T., Carney, B. W., Laird, J. B., & Morse, J. A. 2002, AJ, 124, 1144
Latham, D. W., et al. 2011, ApJ, 732, L24
Lissauer, J. J., et al. 2011, ApJ, accepted (arXiv1102.0543)
Mandel, K., & Agol, E. 2002, ApJ, 580, 171
Meschiari, S., Wolf, A. S., Rivera, E., Laughlin, G., Vogt, S., & Butler, P. 2009, PASP, 121, 1016
Pollacco, D. L., et al. 2006, PASP, 118, 1407
Pollacco, D. L., et al. 2008, MNRAS, 385, 1576
Queloz, D., et al. 2001, A&A, 379, 279
Schneider, J. 2011, http://exoplanet.eu (as of 24 September 2011)
Swain, M, Vasisht, G., & Tinetti, G. 2008, Nature, 463, 637
Tamuz, O., Mazeh, T., & Zucker, S. 2005, MNRAS, 356, 1466
Torres, G. et al. 2007, ApJ, 666, 121
Torres, G., Winn, J. N., & Holman, M. J. 2008, ApJ, 677, 1324
Yi, S. K., Demarque, P., Kim, Y.-C., Lee, Y.-W., Ree, C. H., Lejeune, T., & Barnes, S. 2001, ApJS, 136, 417
Zacharias, N., et al. 2010, AJ, 139, 2184